How do we make an electrostatic loudspeaker with constant directivity?

Tim Mellow[1]

[1] *Mellow Acoustics Ltd, 42 Hale Road, Farnham, Surrey GU9 9QH, UK*

Correspondence should be addressed to Tim Mellow (tim@mellowacoustics.com)

ABSTRACT

The idea of broadening the directivity pattern of a push-pull electrostatic loudspeaker by partitioning the stators into concentric annular rings, which are connected to tappings along a delay line, isn't new. However, the delay line has traditionally been attenuated to avoid response irregularities due to the finite size of the membrane. An alternative approach is presented here whereby a constant-impedance delay line is configured to imitate an oscillating sphere, which is an ideal constant-directivity dipole source that needs no attenuation. Walker's equation for the on-axis pressure does not account for the effect of the delay line without taking the vector sum of the currents though all the rings, so a simple alternative that does is presented here.

1 Introduction

Although there will probably always be a heated debate on exactly what directivity pattern is most desirable for sound reproduction through loudspeakers in an average listening room, one thing there does at least seem to be a consensus on is that the pattern should be as consistent as possible over the entire audio frequency range.[1],[2],[3] In the normal listening position, most of what we hear is reflected sound coming from the off-axis directions. Hence, if the reflected sound does not have the correct tonal balance, it cannot possibly sound natural.

As well as having low coloration and low distortion, electrostatic loudspeakers enable us to control the directivity pattern produced by a single diaphragm in a way which is not possible with dynamic loudspeakers, by partitioning the stators into concentric annular rings which are connected to tappings along a delay line. However, the traditional approach has been to arrange the delay to reproduce the wavefront of a virtual point source located

behind the membrane.[4] Due to the finite size of the membrane, Walker[5] correctly pointed out that the delay line needs to be attenuated to prevent irregularities in the frequency response of the radiated sound. Because the far-field pressure response is the Fourier transform of the sound source, the attenuation may be regarded as a windowing function.

Now imagine a massless sphere oscillating back and forth with constant velocity at all frequencies, thus radiating sound into free space. Such a sound source would have a constant figure-of-eight directivity pattern and at higher frequencies, where the wavelength is smaller than the sphere, constant power would be radiated due to the mainly resistive radiation impedance. Unfortunately, such a sound source is impractical to construct. Even if it were possible to make a large perfectly-rigid hemispherical dynamic driver, it would need a lot of signal boosting at high frequencies to make it move with constant velocity, rather than constant acceleration, and thus radiate constant power. Instead, we shall describe how to imitate an oscillating sphere by using a planar circular

electrostatic loudspeaker with stators partitioned into concentric annular rings which are connected to a delay line.[6] These rings reproduce the sound that would emanate from an oscillating sphere placed immediately behind the membrane (and in contact at the center) as it arrives at the membrane. It turns out that using a geometric approximation that assumes a plane wave travelling axially from the face of the imaginary sphere gives far superior results to reproducing the true magnitude and phase of the waves produced by the sphere. We shall compare the effect of partitioning them into a finite number of rings with equal area, equal delay sections and equal widths, using a continuously varying radial delay as an ideal reference.

For the sake of brevity in a convention paper, we shall ignore secondary effects, such as the membrane mass and stiffness, the stator perforations,[7] and stray capacitances, which are discussed elsewhere,[4] save to mention that membrane mass limits the high frequency response while the stiffness, which is determined by the tension, together with the radiation mass, sets the fundamental resonance frequency. At this frequency, the 1st-order low-frequency roll-off due to the rear-wave cancellation (assuming there is no baffle) becomes a 3rd-order one. Note that the radiation mass is far greater than that of the membrane. The idea here is to describe the main principles of realizing a loudspeaker that imitates an oscillating sphere rather than providing a design cookbook. More details will be given later in the 2nd edition of a book.[8]

2 Construction

A typical electrostatic loudspeaker configuration is shown in Figure 1. In the middle is a light flexible membrane, which is held under tension and clamped at its rim between insulating ring spacers. The spacers separate the membrane from the rigid stators or ring electrodes located either side of it at a distance d. The membrane is circular with a radius a and has a conductive coating which is charged by a polarizing supply with a dc voltage E_P. The polarizing supply is connected via a high-value resistor R_P to prevent the charge on the membrane from varying significantly when the alternating

signal voltage $\tilde{e}_{in}$ is applied to deflect the membrane either side of its central position. We take the input voltage to be that across the entire secondary of a push-pull step up transformer, which is still the most common way to develop the large signal voltage required to drive an electrostatic loudspeaker. As the membrane moves, it produces sound which passes through perforations in the stators. If the loudspeaker is required to produce low frequencies and therefore large membrane excursions, the conductive coating on the membrane is likely to have a high resistance to prevent the charge migrating to the central part which will be closest to the stator at maximum excursion.
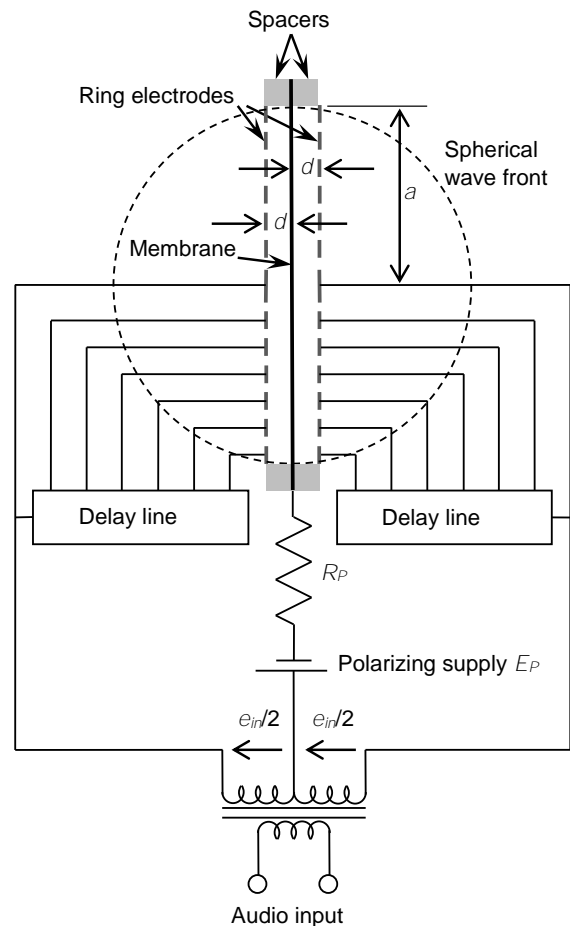

Figure 1. Construction of push-pull electrostatic loudspeaker with delay lines.

Because the membrane is flexible, each part can move more-or-less independently from the rest according to the signal on the nearest ring. Due to the delay line, the sound emanates from the center first, followed by the first ring and then each successive ring in turn until it is radiated from the perimeter, by which time the sound from the center is already some distance away from the membrane. We just need to determine how to configure the delay to produce the optimum wavefront shape.

3 Continuous delay

Let us now consider the ideal situation whereby we increase the number of rings while reducing their widths until the delay becomes continuously variable along the radius of the membrane. Then we can isolate the effect of the delay profile from the discretization of the rings. If we treat the membrane as a pure pressure source with zero mass and stiffness, the far-field radiated sound pressure at a distance r and angle θ from its center is given by inserting the far-field Green's function of Eq. (13.70) from Ref. [8] together with Eq. (13.121) into the dipole boundary integral of Eq. (13.124) from the same reference

$$\tilde{p}(r,\theta) = jk\cos\theta \frac{e^{-jkr}}{r} \\ \times \int_0^a \tilde{p}_+(w)J_0(kw\sin\theta)w\,dw, \qquad (1)$$

where J_0 is the 0$^{\text{th}}$-order Bessel function, $k = \omega/c$ is the wave number, $\omega = 2\pi f$ is the angular frequency, and $\tilde{p}_+(w)$ is the radial distribution of the electrostatic driving pressure. The tilde denotes a harmonically varying quantity where the term $e^{j\omega t}$ has been suppressed.

3.1 No delay

If there is no delay, then the pressure everywhere on the surface of each side is half the driving pressure

$$\tilde{p}_+(w) = \frac{\tilde{p}_0}{2}, \qquad (2)$$

where

$$\tilde{p}_0 = \frac{\varepsilon_0 E_P}{d^2} \tilde{e}_{in}. \qquad (3)$$

and ε_0 is the permittivity of air. Hence, we just have a uniform pressure source or "resilient disk" in free space. The far-field pressure response then becomes

$$\tilde{p}(r,\theta) = ja\frac{\varepsilon_0 E_P}{d^2}\tilde{e}_{in}\frac{e^{-jkr}}{4r}D(\theta), \qquad (4)$$

where the directivity function is given by

$$D(\theta) = \frac{2J_1(ka\sin\theta)}{\sin\theta}\cos\theta. \qquad (5)$$

The directivity pattern $20\log_{10}|D(\theta)| - 20\log_{10}|D(0)|$ is plotted in Figure 2. The on-axis response is simply

$$D(0) = ka, \qquad (6)$$

which is plotted in Figure 7 (black dashed). Note that $D(0)$ here is defined as a dimensionless frequency response function with a constant driving pressure. The input current $\tilde{I}_{in} \approx j\omega C_E \tilde{e}_{in}$ is almost entirely due to the static capacitance $C_E = \varepsilon_0\pi a^2/(2d)$ so that the on-axis pressure simply becomes Walker's equation[5]

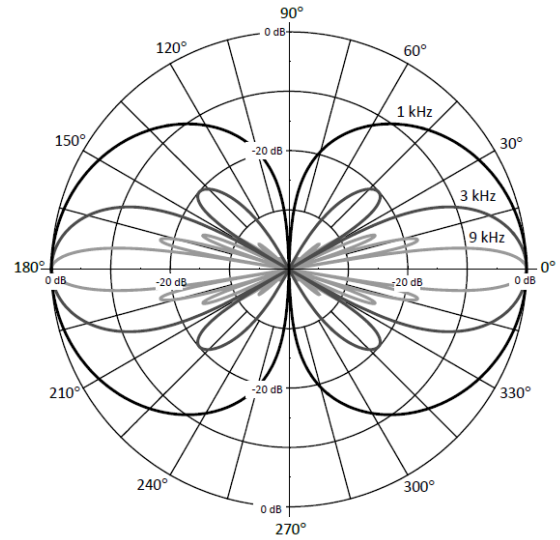
Figure 2. Directivity patterns of 280 mm diameter membrane with no delay. Naturally, the high frequencies are extremely directive.

$$\tilde{p}(r,0) = \frac{E_P}{d} \cdot \frac{e^{-jkr}}{2\pi r} \cdot \frac{\tilde{I}_{in}}{c}. \tag{7}$$

3.2 Virtual point source

The geometry of a traditional "virtual point source" is shown in Figure 3. Due to its finite radius a, the membrane can only reproduce the part of the wavefront emanating from the source which forms a spherical cap with half-angle α and radius of curvature R, where

$$R = a\cot\alpha. \tag{8}$$

To reproduce this, the delay must account for the time taken for the wave to travel the distance ΔR at each point w along the radius according to

$$\Delta R = \sqrt{R^2 + w^2} - R. \tag{9}$$

Hence, the surface pressure distribution is given by

$$\tilde{p}_+(w) = \frac{\tilde{p}_0}{2}e^{jk\Delta R} = \frac{\tilde{p}_0}{2}e^{jk(\sqrt{a^2\cot^2\alpha + w^2} - a\cot\alpha)}, \tag{10}$$

which leads to the directivity pattern

$$D(\theta) = 2ka\cos\theta$$
$$\times \int_0^1 e^{jka(\sqrt{\cot^2\alpha + s^2} - \cot\alpha)} J_0(kas\sin\theta)s\,ds, \tag{11}$$
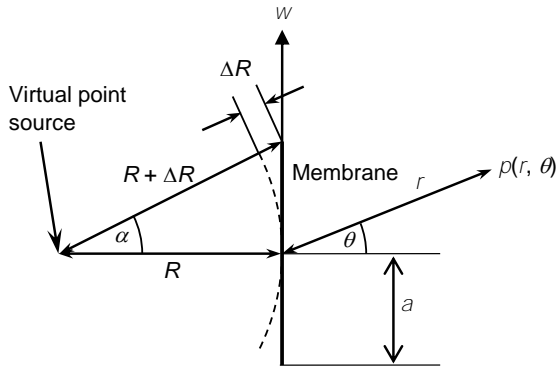

Figure 3. Geometry of virtual point source, which behaves like two back-to-back spherical caps with a discontinuity where they join, unlike a smooth oscillating sphere.
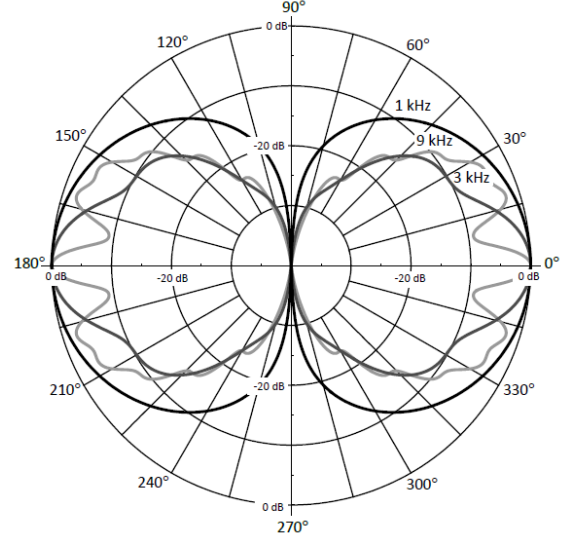

Figure 4. Directivity patterns of virtual point source using a 280 mm diameter membrane, where the half-angle $\alpha = 40°$ is close to that of the Quad ESL63.[4]

where we have substituted $s = w/a$. The directivity pattern $20\log_{10}|D(\theta)| - 20\log_{10}|D(0)|$ is plotted in Figure 4. The on-axis response is

$$D(0) = \frac{2}{ka}$$
$$\times\left(\left(1 - \frac{jka}{\sin\alpha}\right)e^{\frac{jka}{\sin\alpha}} - \left(1 - \frac{jka}{\tan\alpha}\right)e^{\frac{jka}{\tan\alpha}}\right), \tag{12}$$

which is plotted in Figure 7 (dark grey).

3.3 Virtual oscillating sphere

Naïvely, we might insert the pressure produced by an oscillating sphere, given by Eq. (4.129) of Ref. [8], into Eq. (1), while multiplying by $jka/2$ for constant velocity, to yield

$$D(0) = \frac{-k^2a^2}{2 - k^2a^2 + 2jka}\left(e^{-jka} - \frac{e^{-j\sqrt{2}ka}}{\sqrt{2}}\right), \tag{13}$$

where we have substituted $r^2 = w^2 + a^2$ and $\cos\theta = a/r$. The first term in parentheses gives the true response of an oscillating sphere that would be

obtained if the membrane were infinitely large. However, the second term, which is a "diffraction" term due to the membrane's finite size, interferes with the first term to produce an irregular response as shown in Figure 7 (light grey dashed). Hence, for our virtual oscillating sphere, we shall adopt the geometry shown in Figure 5, where the axial distance between each point on the front surface of the virtual sphere and the membrane is $a - \sqrt{a^2 - w^2}$. The amount of delay required at each point along the radius of the membrane is the time taken for sound to travel this distance. Hence,

$$\tilde{p}_+(w) = \frac{\tilde{p}_0}{2} e^{jk(a-\sqrt{a^2-w^2})}, \tag{14}$$
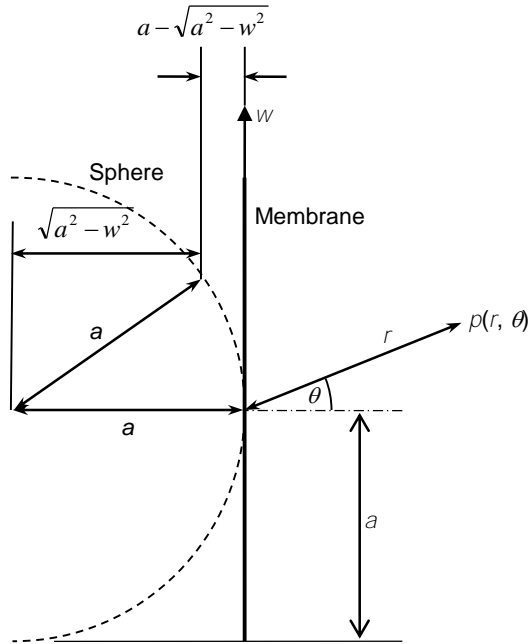
Figure 5. Geometry of virtual oscillating sphere.

which leads to the directivity pattern

$$D(\theta) = 2ka\cos\theta$$
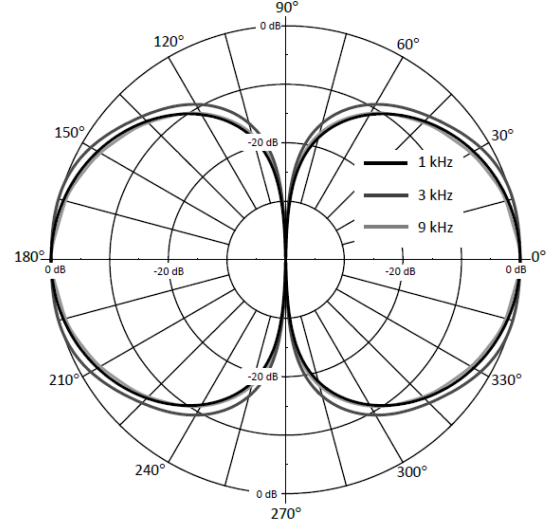$$\times \int_0^1 e^{jka(1-\sqrt{1-s^2})} J_0(kas\sin\theta)s\,ds, \tag{15}$$

Figure 6. Directivity patterns of a virtual oscillating sphere using a 280 mm diameter membrane. The broad figure-of-eight pattern is almost constant at all frequencies.

where we have substituted $s = w/a$. The directivity pattern $20\log_{10}|D(\theta)| - 20\log_{10}|D(0)|$ is plotted in Figure 6. The on-axis response is

$$D(0) = \frac{2}{ka}(1 - e^{jka} + jka), \tag{16}$$

which is plotted in Figure 7 (black) along with the following 1st-order high-pass filter approximation (light grey)

$$D(0) = \frac{2jka}{2 + jka}. \tag{17}$$

This approximation can be included as part of a crossover filter response, for example. The cut-off frequency is given by $f_C = c/(\pi a)$. Above f_C, we have

$$D(0) = 2, \quad f > c/(\pi a). \tag{18}$$

Then from Eqs. (4) and (18) the voltage sensitivity is

$$\tilde{p}(r,0) = j\varepsilon_0 a \frac{E_P}{d} \cdot \frac{\tilde{e}_{in}}{2d} \cdot \frac{e^{-jkr}}{r}, \quad f > \frac{c}{\pi a} \tag{19}$$

and at lower frequencies we have

$$\tilde{p}(r,0) = j\varepsilon_0 ka^2 \frac{E_P}{d} \cdot \frac{\tilde{e}_{in}}{2d} \cdot \frac{e^{-jkr}}{2r}, \quad f < \frac{c}{\pi a} \quad (20)$$

The maximum field strength that we can realistically expect without breakdown is E_P/d = 2000 V/mm. Similarly, the input voltage should not exceed 4000 V peak across 2 mm. If the radius a is 14 cm and the permittivity of free space ε_0 is 8.85 pF/m, the maximum RMS sound pressure from Eq. (19) is 105 dB SPL at 1 m re 20 µPa. This pressure increases by 6 dB for every doubling of the diameter. The on-axis plot of a virtual oscillating sphere shown in Figure 7 tells us that, in theory, a continuously increasing delay in the driving pressure along the radius of the membrane produces a very smooth response, with just some very small ripples, and an almost constant figure-of-eight directivity pattern at all frequencies, as shown in Figure 6. Although perfectly constant directivity is not achieved, the result is remarkably good considering the finite size of the membrane.
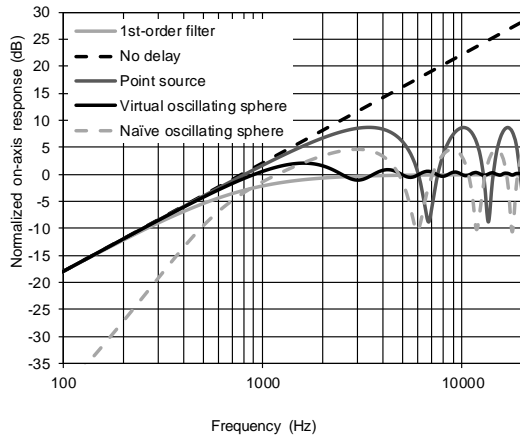

Figure 7. On axis responses $20\log_{10}|D(0)/2|$ of a 280 mm diameter membrane with a continuous and unattenuated delay line configured to simulate an oscillating sphere (black), a naïve oscillating sphere (light grey dashed) and a point source (dark grey) where the half-angle of the arc is 40°. Also shown is a 1st-order filter response that approximates the oscillating sphere (light grey) and the on-axis response of the membrane with no delay (black dashed), which keeps rising as the energy is focused on-axis.

4 Effect of discretization into rings of finite width

4.1 Rings of equal delay

One option might be to vary the widths of the rings so that there are equal delay sections between them, in which case the on-axis pressure is

$$D(0) = ka \sum_{n=0}^{N} e^{-jka\frac{n+1/2}{N+1}} \left(\frac{a_n^2 - a_{n-1}^2}{a^2} \right) \quad (21)$$

where the radius of the nth ring is

$$a_n = a\sqrt{1 - \left(1 - \frac{n+1}{N+1}\right)^2}, \quad (22)$$

a_0 is the radius of the center disk and $a_{-1} = 0$. In Eq. (21), the term in parentheses is proportional to the area of the nth ring while the exponent term represents the delay applied to that ring. The cross-section of a stator with rings of equal delay is shown in Figure 8.
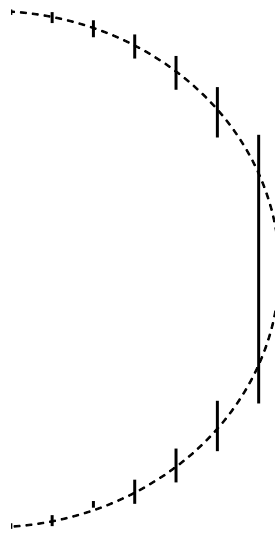

Figure 8. Cross-section of stator divided into concentric rings of *equal delay*, where purely for illustration each ring has been shifted to the left by the distance that a wave would have travelled during the time delay applied to that ring.

4.2 Rings of equal area

Another option might be to vary the widths of the rings so that they all have the same area and capacitance, in which case the on-axis pressure is

$$D(0) = ka \sum_{n=0}^{N} e^{-jka\left(1-\sqrt{1-\frac{a_{n-1/2}^2}{a^2}}\right)} \left(\frac{a_n^2 - a_{n-1}^2}{a^2}\right), \qquad (23)$$

where the radius of the nth ring is

$$a_n = a\sqrt{\frac{n+1}{N+1}}. \qquad (24)$$

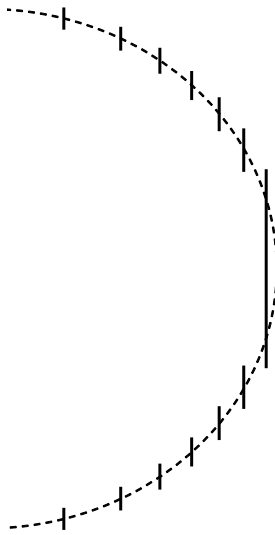The cross-section of a stator with rings of equal delay is shown in Figure 9.

Figure 9. Cross-section of stator divided into concentric rings of *equal area*, where purely for illustration each ring has been shifted to the left by the distance that a wave would have travelled during the time delay applied to that ring.

4.3 Rings of equal width

The last option we shall consider is one in which the rings are of equal width, in which case the on-axis pressure is again given by Eq. (23) but with the radius of the nth ring given by

$$a_n = a\frac{n+1}{N+1}. \qquad (25)$$

The cross-section of a stator with rings of equal delay is shown in Figure 10 while the on-axis responses with equal delay, equal area and equal width are plotted in Figure 11.

Figure 10. Cross-section of stator divided into concentric rings of *equal width*, where purely for illustration each ring has been shifted to the left by the distance that a wave would have travelled during the time delay applied to that ring.
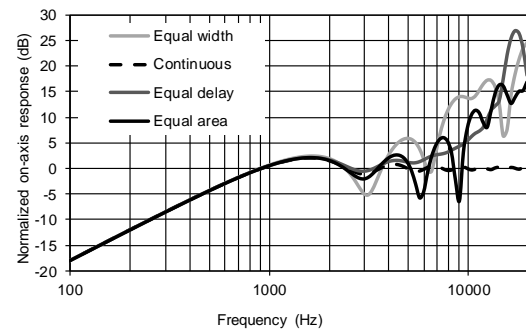

Figure 11. Effects of discretization on a 280 mm diameter membrane where the stator is divided into 6 rings and a center disk of various widths with the delay configured to simulate an oscillating sphere.

Arguably, the rings of equal delay produce the smoothest response at the higher frequencies due to their finer resolution of the rapid increase in delay near the rim, as shown in Figure 8. However, the outer rings are so thin that stray capacitances will dominate the ring capacitances, whereas a stator with rings of equal width largely avoids this problem. Also, the wide center disk will produce high-frequency beaming. Hence, the stator with rings of equal width, as shown in Figure 10, is the most useful in practice because a real delay line that rolls off the sound from the outermost rings first will smooth out the response in all directions, as we shall see. If the rings have equal width, they can be narrower than the wavelength over most the audio spectrum.

5 A practical delay line

We saw in the last section that the discretization of the delay into rings of finite width produces irregularities in the response at higher frequencies. However, the delay was an ideal delay like that produced by a DSP, whereas in practice, the delay is more likely to take the form of an analogue delay line on the high-voltage side of the transformer, such as that shown in Figure 12. Otherwise, a separate stepping up transformer would be needed to feed

each ring. Unless complicated inductors with center taps or a very large number of inductors are used, analogue delay lines tend to introduce a degree of attenuation at the higher frequencies. In this case, this turns out to have a smoothing effect on the response. From Figure 5, we see that the *total* delay path-length z_T at each point along the radial ordinate w is given by

$$z_T = a - \sqrt{a^2 - w^2} = a\left(1 - \sqrt{1 - \frac{w^2}{a^2}}\right). \qquad (26)$$

For discretized rings, the delay section z_n required for the nth ring is the difference between the total delay z_{Tn} at that ring and the sum of all the previous delay sections

$$z_n = z_{Tn} - \sum_{m=1}^{n-1} z_m, \qquad (27)$$

where

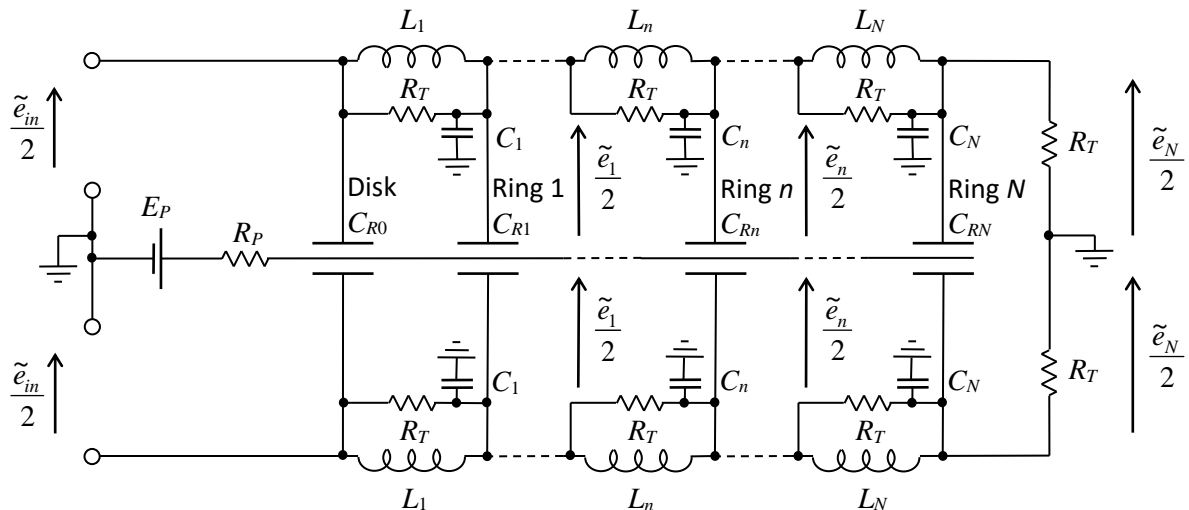$$z_{Tn} = a\left(1 - \sqrt{1 - \left(\frac{a_{n-1} + a_n}{2a}\right)^2}\right). \qquad (28)$$

Figure 12. Constant-impedance delay line.

Notice that we have taken the delay path to the midpoint $(a_{n-1} + a_n)/2$ of each ring. The nth path-length z_n is related to the time delay T_n of the nth section by

$$z_n = cT_n, \tag{29}$$

where c is the speed of sound. In Figure 12, C_{Rn} are the ring capacitances which are given by

$$C_{Rn} = \frac{\varepsilon_0 \pi (a_n^2 - a_{n-1}^2)}{2d} \tag{30}$$

$$C_{R0} = \varepsilon_0 \pi a_0^2 /(2d) \tag{31}$$

while C_n are shunt capacitors used to make up the required capacitance for the correct delay and impedance. The delay line comprises inductors L_n together with the total capacitances of each section

$$C_{Tn} = C_{Rn} + C_n / 2 \tag{32}$$

where R_T is the termination resistance on the far right-hand side. The termination resistance is also connected across each inductor to create a series of Zobel networks such that the impedance presented to the preceding section is always $2R_T$. The voltage transfer function of each delay section is given by

$$\frac{\tilde{e}_n}{\tilde{e}_{n-1}} = \frac{\omega_n}{s + \omega_n} \tag{33}$$

provided that the inductor values are set to

$$L_n = 2R_T^2 C_{Tn}, \tag{34}$$

where $s = j\omega$ and

$$\omega_n = \frac{1}{2R_T C_{Tn}}. \tag{35}$$

The time delay T_n per section is defined by

$$T_n = \frac{z_n}{c} = \frac{1}{\omega_n} = 2R_T C_{Tn} = \frac{L_n}{R_T}. \tag{36}$$

so that the total capacitance per section is given by

$$C_{Tn} = \frac{z_n}{2cR_T}. \tag{37}$$

We can now furnish each section of the delay with its respective component values

$$C_n = 2(C_{Tn} - C_{Rn}) \tag{38}$$

where C_{Tn} is given by Eq. (37) and C_{Rn} by Eq. (30). From Eq. (36) we have

$$L_n = \frac{z_n R_T}{c}. \tag{39}$$

We wish to minimize the capacitor values so that most of the signal current flows through the rings. If we set $C_1 = 0$ so that $C_{T1} = C_{R1}$, then

$$R_T = \frac{z_1}{2cC_{R1}}. \tag{40}$$

Each delay section is represented by the transmission matrix

$$\begin{bmatrix} \tilde{e}_{n-1} \\ \tilde{i}_{n-1} \end{bmatrix} = \mathbf{A}_n \cdot \begin{bmatrix} \tilde{e}_n \\ \tilde{i}_n \end{bmatrix} \tag{41}$$

where

$$\mathbf{A}_n = \begin{bmatrix} a_{11}(n) & a_{12}(n) \\ a_{21}(n) & a_{22}(n) \end{bmatrix} \tag{42}$$

and each element of $\mathbf{A}_n$ is given by

$$a_{11}(n) = \left.\frac{\tilde{e}_{n-1}}{\tilde{e}_n}\right|_{\tilde{i}_n=0} = 1 + 2\frac{sL_n R_T}{sL_n + R_T} sC_{Tn}, \tag{43}$$

$$a_{12}(n) = \left.\frac{\tilde{e}_{n-1}}{\tilde{i}_n}\right|_{\tilde{e}_n=0} = 2\frac{sL_n R_T}{sL_n + R_T}, \tag{44}$$

$$a_{21}(n) = \left.\frac{\tilde{i}_{n-1}}{\tilde{e}_n}\right|_{\tilde{i}_n=0} = sC_{Tn}, \tag{45}$$

$$a_{22}(n) = \left.\frac{\tilde{i}_{n-1}}{\tilde{i}_n}\right|_{\tilde{e}_n=0} = 1. \tag{46}$$

However, the first section contains no inductor, only the capacitance of the center disk

$$\mathbf{A}_0 = \begin{bmatrix} 1 & 0 \\ sC_{R0} & 1 \end{bmatrix}. \tag{47}$$

Hence, we can describe the whole delay line of Figure 12 by multiplying together the chain matrices

$$\begin{bmatrix} \tilde{e}_{in} \\ \tilde{i}_{in} \end{bmatrix} = \mathbf{A}_0 \cdot \mathbf{A}_1 \cdots \mathbf{A}_N \cdot \begin{bmatrix} 1 & 0 \\ (2R_T)^{-1} & 1 \end{bmatrix} \cdot \begin{bmatrix} \tilde{e}_N \\ 0 \end{bmatrix}$$

$$= \mathbf{A} \cdot \begin{bmatrix} \tilde{e}_N \\ 0 \end{bmatrix} = \begin{bmatrix} a_{11} & a_{12} \\ a_{21} & a_{22} \end{bmatrix} \cdot \begin{bmatrix} \tilde{e}_N \\ 0 \end{bmatrix} \qquad (48)$$

where $\tilde{e}_{in}$ and $\tilde{i}_{in}$ are the input voltage and current respectively and $\tilde{e}_N$ is the voltage across the termination impedance $2R_T$. We evaluate $\tilde{e}_N$ from

$$\tilde{e}_N = \tilde{e}_{in} / a_{11}. \qquad (49)$$

The then voltage and current at the junction of each section may be calculated by working back from the termination

$$\begin{bmatrix} \tilde{e}_n \\ \tilde{i}_n \end{bmatrix} = \mathbf{A}_{n+1} \cdot \mathbf{A}_{n+2} \cdots \mathbf{A}_N \cdot \begin{bmatrix} 1 & 0 \\ 1/(2R_T) & 1 \end{bmatrix} \cdot \begin{bmatrix} \tilde{e}_N \\ 0 \end{bmatrix}. \qquad (50)$$

Hence the driving pressure produced by each ring is

$$\tilde{p}_n = \frac{\varepsilon_0 E_P}{d^2} \tilde{e}_n \qquad (51)$$

$$\tilde{p}_0 = \frac{\varepsilon_0 E_P}{d^2} \tilde{e}_{in} \qquad (52)$$

6 Far-field sound pressure

The far-field pressure is derived in the same way as that for a resilient disk in free space [11] and is the sum of the pressures radiated from each individual ring

$$\tilde{p}(r,\theta) = -ja\tilde{p}_0 \frac{e^{-jkr}}{4r} D(\theta) \qquad (53)$$

where $D(\theta)$ is the directivity function given by

$$D(\theta) = \frac{2}{a} \cot\theta \left(a_0 J_1(ka_0 \sin\theta) + \sum_{n=1}^{N} \frac{\tilde{p}_n}{\tilde{p}_0} \right.$$
$$\left. \times \left(a_n J_1(ka_n \sin\theta) - a_{n-1} J_1(ka_{n-1} \sin\theta) \right) \right), \qquad (54)$$

which is plotted in Figure 13. The on-axis response is given by

$$D(0) = \frac{ka_0^2}{a} + \sum_{n=1}^{N} \frac{\tilde{p}_n k(a_n^2 - a_{n-1}^2)}{\tilde{p}_0 a}, \qquad (55)$$

which is plotted in Figure 14 using the quantities given in Table 1, where the total delay is 255 μs and the width of each ring is 2 cm.

Parameters	Resistor & constants	Inductors	Capacitors	Turnover frequencies
a = 140 mm	R_T = 282 kΩ	L_1 = 2.66 H	C_1 = 0 pF	f_1 = 16.9 kHz
d = 1 mm	ρ_0 = 1.18 kg/m^3	L_2 = 4.90 H	C_2 = 5.75 pF	f_2 = 9.18 kHz
r = 1 m	c = 345 m/s	L_3 = 7.80 H	C_3 = 20.0 pF	f_3 = 5.77 kHz
$e_{in} = 2\sqrt{2}$ kV$_{rms}$	ε_0 = 8.85 pF/m	L_4 = 11.5 H	C_4 = 43.6 pF	f_4 = 3.92 kHz
E_P = 2 kV		L_5 = 16.9 H	C_5 = 89.4 pF	f_5 = 2.66 kHz
N = 6		L_6 = 28.4 H	C_6 = 211 pF	f_6 = 1.59 kHz

Table 1. Quantities used in calculation of directivity patterns shown in Figure 13 and on-axis response shown in Figure 14 for a of a 280 mm diameter membrane discretized into 6 equal rings and center disk using the delay line of Figure 12 with 6 sections.
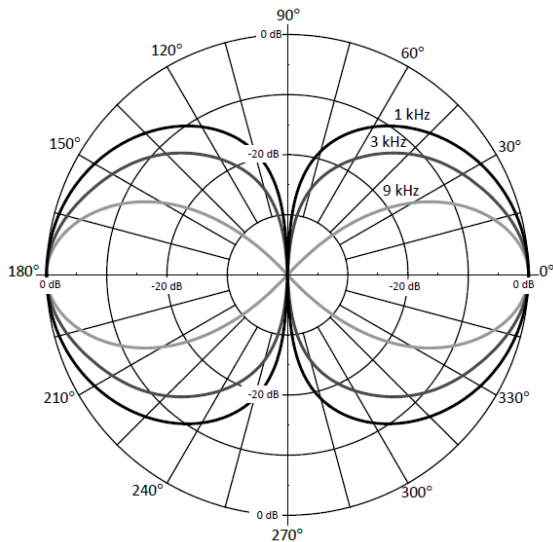
Figure 13. Directivity patterns of a 280 mm diameter membrane discretized into 6 equal rings and center disk using the delay line of Figure 12 with 6 sections
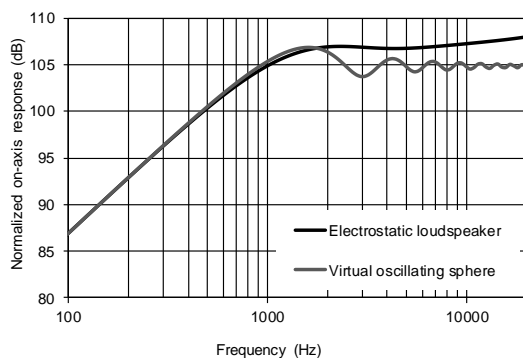

Figure 14. On axis responses of a 280 mm diameter membrane with the delay configured to simulate an oscillating sphere where the delay is continuous (grey) and discretized into 6 equal rings and center disk (black) using the delay line of Figure 12.

7 Conclusions

We have shown that when the delay line of an electrostatic loudspeaker is configured so that it imitates an oscillating sphere, it is not the delay line but the discretization of the stator into rings of finite

width that produces irregularities in the pressure response of Figure 11. However, a very smooth response may be obtained using an analogue delay line, as shown in Figure 14. Although this doesn't produce a constant directivity pattern up to the very highest frequencies, broad directivity is maintained throughout the vital midrange and lower treble, as shown in Figure 13. Equation (19) is a useful formula for the voltage sensitivity when such a delay line is used, although Walker's Equation (20) still applies for $f < c/(\pi a)$.

References

[1]   Floyd E. Toole, "Music, Rooms and Listeners: Science in the Creation and Delivery of Audio Art," Acoustics Today **9**(2), 36–44 (2013) http://acousticstoday.org/issues/2013AT/Apr2013/#?page=36.

[2]   S. Linkwitz, "The Magic in 2-Channel Sound Reproduction - Why is it so Rarely Heard?," Int. J. Archit. Eng. Technol. **2**, 113-126 (2015) http://www.linkwitzlab.com/IJAETv2n2a2-Linkwitz-1.pdf.

[3]   J. Watkinson, "We need to talk about Speakers: Sorry, 'audiophiles', only IT will break the sound barrier," The Register, 2nd July (2014). http://www.theregister.co.uk/2014/07/02/feature_the_future_loudspeaker_design/?page=1

[4]   J. Borwick, *Loudspeaker and Headphone Handbook*, 3rd ed. (Focal, Oxford, 2001), pp. 108-195.

[5]   P. J. Walker, "New Developments in Electrostatic Loudspeakers," J Audio Eng. Soc. **28**(11), 795–799 (1980).

[6]   T. J. Mellow, and L. M. Kärkkäinen, "A dipole loudspeaker with a balanced directivity pattern," J. Acoust. Soc. Am. **128**(5), 2749-2757 (2010).

[7]   D. R. White and S. Bolser, " Acoustic Transparency of Electrostatic Loudspeaker Assemblies," J Audio Eng. Soc. **65**(6), 497−506 (2017).

[8]   L. L. Beranak and T. J. Mellow, *Acoustics: Sound Fields and Transducers*, 1st Ed. Academic Press, Oxford (2012), pp. 548 and 563.